Mechanism of Charge Recombination in Dye-Sensitized Nanocrystalline Semiconductors: Random Flight Model

A. V. Barzykin and M. Tachiya*

National Institute of Advanced Industrial Science and Technology, Tsukuba, Ibaraki 305-8565 Japan

Received: August 1, 2001; In Final Form: February 11, 2002

The trap-filling effect on the kinetics of charge recombination in dye-sensitized TiO_2 nanoparticles is discussed on the basis of the random flight model. The model assumes that electrons move between trap sites on the surface of a nanoparticle by diffusion in the conduction band. After an electron is thermally detrapped into the conduction band, it can subsequently be captured by any empty trap or recombine with a cation within the same nanoparticle. This is an alternative to the nearest-neighbor random walk. A reasonable agreement with recent experimental data is observed. It is concluded, in accord with the previous studies, that the reaction is governed by the energy redistribution of trapped electrons rather than by spatial diffusion.

I. Introduction

The interfacial charge-transfer kinetics of dye-sensitized nanocrystalline semiconductors, such as TiO_2, has received a great deal of current attention, mainly because of recent developments in photovoltaic devices.[1] Electron injection from the photoexcited state of a dye into the conduction band of a semiconductor is typically over within a picosecond and the kinetics of this process was found to be rather insensitive to variations in experimental conditions.[2] On the other hand, charge recombination between the dye cation and the injected electrons was observed to occur nonexponentially over picosecond-millisecond time scales.[3,4] Recent experimental findings indicate that the recombination rate depends on the intensity of the light source as well as on the concentration of dark electrons introduced into the semiconductor by externally applied bias or by changing the surrounding electrolyte composition.[4] The wide range of time scales is usually attributed to the trapping of electrons by localized states on the semicondictor surface.[4−9] Nanocrystalline materials, possessing a high surface area, have been widely reported to have a high density of such trap states.[1b] Experiments show that the recombination rate strongly depends on the occupancy of the trap levels, so strongly that the application of an external negative potential of only 500 mV results in a nearly 10^7-fold acceleration of the kinetics.[4] This nonlinear behavior is inconsistent with the usual second-order kinetic models of recombination and suggests that the reaction is controlled by electron transport between energetically distributed trap sites.

Since the kinetics of charge recombination is critical to the efficiency of the device, it is important to correlate it with the density and nature of the trap states. Several models of charge transport and recombination have been developed.[5−11] The starting point in the analysis is that the transport is diffusive, that is, there are no macroscopic electric fields across the sample because of the screening effect of the electrolyte. In fact, transient and steady-state photocurrent measurements were often interpreted in terms of the diffusion equation for the carrier density with additive volume generation and recombination terms.[6] However, this can be done only with a certain reservation because an apparent diffusion coefficient turns out to be dependent on the carrier density.[7,12] In conventional semiconductor theory, there are two models of dispersive transport which implicitly include the distribution of intraband gap states: the multiple-trapping (MT) model[13−15] and the continuous-time random walk (CTRW) model.[16,17] In the limit of low-carrier density, these two models were proven to be mathematically equivalent.[13] They predict a power law behavior for the photocurrent transient and a stretched-exponential asymptotic behavior for the survival probability of charge carriers in the presence of recombination, as a consequence of the exponential distribution of the density of localized states below the conduction band.

Nelson has recently applied the CTRW model to experimental situations of transient photocurrent and charge recombination in a Monte Carlo simulation study, emphasizing the importance of the trap-filling effect.[10a] Although the model was rather idealistic (nearest-neighbor walk on an infinite cubic lattice), it showed a reasonable agreement with recent experimental results of Haque et al.[4a] Certain questions still remain. First, it is known that the long-time behavior of the survival probability is sensitive to the dimensionality of the embedding space, and the traps are most likely distributed on 2D surfaces rather than homogeneously within the 3D medium. Second, the characteristic thermal detrapping time of 5 fs she obtained by fitting the experimental decay data appears to be too fast.

In their very recent work,[10b] Nelson et al. have employed the MT model assuming that electrons leave traps by full thermal activation up to the conduction band and that they can be retrapped only by the nearest-neighboring traps. Good agreement with experimental cation absorption decay data as a function of applied bias has been achieved, which is particularly remarkable because the initial electron number density per nanoparticle was not a fitting parameter — it was estimated on the basis of a spectral measurement. The effect of trap distribution on a 2D spherical shell compared to a 3D medium has also been considered and it was concluded that this effect is minor, that is, the kinetics is dominated by the energetic distribution of trap states rather than the geometry. The nearest-

* To whom correspondence should be addressed.

10.1021/jp012957+ CCC: $22.00
Published on Web 04/06/2002

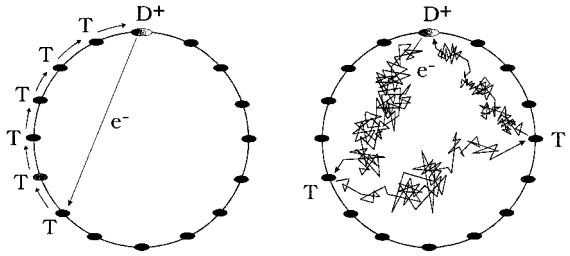

Figure 1. Two models of charge recombination in a semiconductor nanoparticle. In both cases cations are immobile, while electrons can move between trap sites on the surface of the nanoparticle by thermal activation to the conduction band. The model of Nelson et al.[10b] is shown on the left and corresponds to the nearest-neighbor random walk. In the original formulation,[10a] Nelson considered the walk on an infinite 3D cubic lattice. Our model is shown on the right and corresponds to a completely random choice of the next trapping site for an electron within the nanoparticle after its detrapping and diffusion in the condiction band.

neighbor hopping may also imply electron tunneling, with the activation energy depending on the energies of the initial and final trap sites. Nelson et al. have shown that the MT nearest-neighbor model describes the shape of the kinetic curves better and thus ruled out the possibility of tunneling via the Miller−Abrahams mechanism.[18]

Since the trap sites in semiconductor nanoparticles are usually located on their surface while the conduction band should normally be associated with their inner part, it is hard to accept without doubt that an electron, once activated up to the conduction band, will be captured just by the neighboring trap. Instead, in the spirit of the MT formulation where the driving force for spatial motion of charge carriers is their concentration gradient in the conduction band, it seems more reasonable to assume that there is a certain probability for an electron to move a certain distance within the nanoparticle before it is trapped again. The distribution of distance the electron travels from the original trap site on the surface to the next one should depend on the ratio of the trapping rate constant and the diffusion coefficient D in the conduction band. If this ratio is large, the distribution is close to a delta function and the nearest-neighbor mechanism is realized. In the opposite limit, the distribution is broad and ultimately one is led to the random flight model, where the probability for the detrapped electron to be captured by any empty surface trap within the nanoparticle is the same (see Figure 1). Since the quoted value of D for bulk (rutile) TiO_2 is rather high, 1.5×10^{-6} m^2 s^{-1} (ref 19), we can take it as a certain evidence (not a proof) in favor of the latter mechanism.

In this paper, we will consider the random flight model and try to mimic the experimental situation of charge recombination in TiO_2, as observed by Haque et al.[4] We will assume that (a) since the number of carriers in these experiments is sufficiently high (more than one per nanoparticle), recombination is mainly an intraparticle event; (b) the electron density in the conduction band is negligible; (c) the capture cross section is the same for all traps and cations (since we do not know otherwise); and (d) as soon as any electron is thermally detrapped into the conduction band, it can subsequently be captured by any empty trap or recombine with a cation with equal probability. Basically, only (d) is different from the model studied by Nelson et al.[10] The advantage of this very simple model is that it can be readily analyzed both numerically and even analytically. Also, as we shall see, it already shows a reasonable agreement with the experimental data making us conclude, in accord with the previous studies, that the reaction is mainly governed by the energy redistribution of trapped electrons rather than by spatial diffusion.

II. The Model

A. Effect of Light Intensity. Consider a nanoparticle with N electron trap sites and assume a sufficiently low Fermi energy level so that all traps are vacant. This is a reasonable assumption for unbiased experiments. As it can be estimated from the natural doping density of TiO_2, the average number of electrons per 10 nm radius particle in the dark is only 0.1, while the number of trap sites N is quoted to be several hundred.[20] Pulsed excitation of the dye-sensitized TiO_2 leads to formation of the dye cation state which is then re-reduced by charge recombination with photogenerated electrons. Experimentally, one monitors the decay kinetics of the cation state. Let $n(t)$ be the number of photogenerated cations at time t and hence also the number of photogenerated electrons. We assume that the electrons are rapidly trapped and their concentration in the conduction band is negligible. The energy distribution of electron trap states $g(E)$ is taken to be exponential below the conduction band,

$$g(E) = \alpha/k_B T \exp(-\alpha E/k_B T) \quad (1)$$

Here, the conduction-band edge energy is set to zero. If the carriers leave the trap sites by thermal activation, the corresponding detrapping rate constant is given by

$$k_d(E) = k_d^0 \exp(-E/k_B T) \quad (2)$$

where k_d^0 is determined by the thermal frequency of the semiconductor. According to detailed balance, k_d^0 gives the rate of capture of a conduction band electron by a vacant trap.

Our model scenario of charge recombination is as follows. Initially, electrons are distributed among traps at random, that is, according to $g(E)$. When any one electron is thermally detrapped into the conduction band, it has an equal chance to be captured by an empty trap or to recombine with any of the cations within the same nanoparticle. For the time being, we neglect interparticle migration of electrons. This random flight formulation assumes nonequilibrium. As we shall see below, the true equilibrium Fermi distribution is established only at the later stage of the kinetics because the equilibration process (trapping−detrapping) competes with recombination. One can easily extend this model to the situation where the rate of recombination is different from the trapping rate, if there is an experimental evidence for this.

1. Simulation Details.

Our simulation strategy is based on Monte Carlo sampling. It is very similar to the method used by Nelson et al. in ref 10b. We begin by choosing N trap energy levels E_i according to the distribution $g(E)$ and placing initially produced $n_0 = n(0)$ electrons at random onto n_0 of these levels. A trap can accommodate only one electron. n_0 is determined by the excitation pulse intensity. Then we generate detrapping times t_i for all electrons on the basis of the corresponding waiting time distribution functions,

$$\psi_i(t) = k_d(E_i) \exp[-k_d(E_i)t] \quad (3)$$

Now, an electron with the shortest detrapping time $t_j = \min(t_i)$ is detrapped, the current time is advanced by t_j, and the detrapping times for the rest of the electrons are updated, $t_i = t_i - t_j$ $(i \neq j)$. The fate of the freed electron is decided immediately; it is placed at random either on one of $N - n +$

1 vacant trap sites or on one of n cations. In case the freed electron is retrapped, it is assigned a new detrapping time t_j in accordance with its new trap energy level E_j. t_j is added to the updated set of t_i, and a new electron with the shortest detrapping time is selected. As soon as the freed electron reaches a cation, they annihilate, n is decreased by 1, and the corresponding time moment is recorded. Next, an electron with the shortest detrapping time is picked from the surviving set of electrons, and the procedure is continued in this fashion until no electron is left. The survival probability,

$$P(t) = n(t)/n_0 \tag{4}$$

is obtained as an average over many trajectories (10^4 has proven to be sufficient for convergence).

2. Approximate Analytical Solution. Since the number of traps per TiO_2 nanoparticle is typally large (over 500), we may consider a thermodynamic limit of the above model as a useful approximation. From now on we will use dimensionless units of time, $\tau = k_d^0 t$, and energy, $\epsilon = E/k_B T$. By assuming a quasistationary state for electrons in the conduction band, one can write the following nonlinear integro-differential master equation for the distribution function $f(\epsilon,\tau)$ of trapped electrons,

$$\frac{\partial}{\partial\tau} f(\epsilon,\tau) = -e^{-\epsilon} f(\epsilon,\tau) + \frac{N\, g(\epsilon) - f(\epsilon,\tau)}{N} \int_0^\infty d\epsilon\, e^{-\epsilon} f(\epsilon,\tau) \tag{5}$$

with the initial condition, $f(\epsilon, 0) = n_0 g(\epsilon)$. The meaning of eq 5 is quite clear: the first term on the right-hand side corresponds to detrapping, while the second term represents the total detrapping rate multiplied by the density of vacant traps. The time-dependent number density $n(\tau)$ of electrons (cations) is given by the integral of the distribution function over energy,

$$n(\tau) = \int_0^\infty d\epsilon\, f(\epsilon,\tau) \tag{6}$$

The kinetic equation for $n(\tau)$ reads,

$$\frac{1}{n}\frac{dn}{d\tau} = -\frac{1}{N}\int_0^\infty d\epsilon\, e^{-\epsilon} f(\epsilon,\tau) \tag{7}$$

By introducing the normalized distribution function, $f(\epsilon,\tau)/n(\tau)$, eq 5 can be linearized and solved (see Appendix). We obtain for the survival probability,

$$P^{-1}(\tau) = 1 + (n_0/N)\, K(\tau) \tag{8}$$

Here the Laplace transform of $K(\tau)$ is given by

$$\hat{K}(s) \equiv \int_0^\infty d\tau\, e^{-s\tau} K(\tau) = \frac{1}{s}\left[\frac{1}{h(s)} - 1\right] \tag{9}$$

with

$$h(s) = {}_2F_1(1, \alpha; 1+\alpha; -1/s) \tag{10}$$

where ${}_2F_1$ is the hypergeometric function. Inverse Laplace transformation can be readily evaluated numerically.

Equation 8 can be considerably simplified if one takes into account that n_0 is typically $\ll N$ and hence $P(\tau)$ will deviate from unity somewhat noticeably only in the long-time limit corresponding to $s \to 0$. In this limit,

$$h(s) = s^\alpha\, \pi\alpha\, \csc(\pi\alpha) + \mathcal{O}(s) \tag{11}$$

leading to

$$P^{-1}(\tau) = 1 + (n_0/N)\, c\tau^\alpha \tag{12}$$

where $c = [\pi\alpha\, \csc(\pi\alpha)\, \Gamma(1+\alpha)]^{-1}$ and $\Gamma(x)$ is the gamma function. As we shall see below, this type of behavior should be expected in the low concentration limit for any mechanism of migration (nearest-neighbor walk or random flight). All information about the mechanism, spatial configuration and the number of trap sites, will be contained in the proportionality constant c.

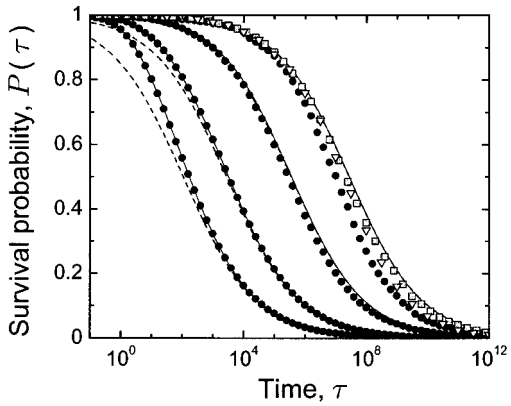

Figure 2. Cation survival probability $P(\tau)$ as a function of reduced time $\tau = k_d^0 t$ for a different initial number density of photogenerated electrons and cations, $n_0/N = 0.002$, 0.01, 0.06, 0.2 (right to left), in the absence of dark electrons. The trap energy distribution is exponential with $\alpha = 0.39$. Circles are Monte Carlo results for $N = 500$ trap sites per nanoparticle, solid lines represent the solution in the thermodynamic limit (eq 8, where Laplace inversion was performed numerically using the Crump algorithm), and dashed lines describe the low-density approximation (eq 12). Triangles and squares are simulation results for $N = 1000$ ($n_0 = 2$) and $N = 2000$ ($n_0 = 4$), respectively.

3. Numerical Results. Figure 2 compares the simulated decay curves for $N = 500$ against analytical solution in the thermodynamic limit for several values of the initial electron number density. The agreement is seen to be quite reasonable. Deviations due to finite-size effects at low densities practically disappear as N is increased to 2000. The accuracy of eq 12 turns out to be very good (with respect to the exact solution in the thermodynamic limit). Only for n_0/N as high as 0.1 the discrepancy at short times becomes substantial. Given that the model itself is quite idealistic, this simple approximate solution could be quite useful for estimations.

B. Effect of Applied Bias. Applied bias changes the electron Fermi level. The higher this level is, the larger is the number of dark electrons occupying trap sites prior to photoexcitation. Dark electrons are at thermal equilibrium. The number density of dark electrons n_d is related to the Fermi energy $\epsilon_F = E_F/k_B T$ as follows:

$$n_d = \int_0^\infty d\epsilon\, g_F(\epsilon) \tag{13}$$

in accordance with the Fermi statistics. Here we have denoted,

$$g_F(\epsilon) = \frac{N\, g(\epsilon)}{1 + \exp(\epsilon_F - \epsilon)} \tag{14}$$

The model scenario of charge recombination is quite similar to case A, the only difference being that some of the low-level trap sites are now preoccupied by dark electrons which can also participate in the reaction.

1. Simulation Details. As before, we start our simulation by choosing N trap energy levels E_i from the distribution $g(E)$. Then we populate these levels with thermal electrons according to the Fermi probability, $(1 + \exp[(E_F - E_i)/k_BT])^{-1}$. The total number of dark electrons n_d is obtained by summation for each run. Then we place $n_0 = n(0)$ photogenerated electrons completely at random onto n_0 of the vacant trap levels. The rest of the simulation scheme is basically the same. Again, we monitor the time evolution of the number $n(t)$ of cations, which is now different from (less than) the total number of electrons, $n_t(t) = n(t) + n_d$.

2. Approximate Analytical Solution. In the thermodynamic limit, the master equation for the distribution function of trapped electrons reads,

$$\frac{\partial}{\partial\tau} f(\epsilon, \tau) = - e^{-\epsilon} f(\epsilon, \tau) + \frac{N\, g(\epsilon) - f(\epsilon, \tau)}{N - n_d} \int_0^\infty d\epsilon\, e^{-\epsilon} f(\epsilon, \tau) \quad (15)$$

with the initial condition,

$$f(\epsilon, 0) = n_0 \frac{N\, g(\epsilon) - g_F(\epsilon)}{N - n_d} + g_F(\epsilon) \quad (16)$$

Integration over energy gives us the kinetic equation for the number density of photogenerated electrons (cations),

$$\frac{1}{n}\frac{dn}{d\tau} = - \frac{1}{N - n_d} \int_0^\infty d\epsilon\, e^{-\epsilon} f(\epsilon, \tau) \quad (17)$$

which essentially coincides with eq 7, but now $f(\epsilon, \tau)$ is the full distribution function including dark electrons.

As before, we linearize the master equation by introducing the auxiliary distribution function, $f(\epsilon, \tau)/n(\tau)$. Finally, the solution is obtained in the form (see Appendix)

$$P^{-1}(\tau) = \exp(\tau\, e^{-\epsilon_F}) + (n_0/N)\, K(\tau) \quad (18)$$

where $K(\tau)$ is now given by

$$K(\tau) = \mathcal{L}^{-1}\left[\frac{1}{s}\frac{N}{N\, h(s) - n_d}\right] - \frac{N}{N - n_d} \exp(\tau\, e^{-\epsilon_F}) \quad (19)$$

Here $\mathcal{L}^{-1}$ denotes inverse Laplace transformation. A simple approximation can be derived by taking into account that usually both n_0 and n_d are $\ll N$. We obtain

$$P^{-1}(\tau) = \exp(\tau\, e^{-\epsilon_F}) + (n_0/N)\, c\, \tau^\alpha \quad (20)$$

as a natural generalization of eq 12. All the parameters were defined earlier. The first term on the right-hand side of eq 20 shows the effect of dark electrons, while the second term can be ascribed to photogenerated electrons.

3. Numerical Results. Figure 3 compares the simulated decay curves for $N = 500$ against analytical solution in the thermodynamic limit for $n_0 = 1$ ($n_0/N = 0.002$) and several values of Fermi energy. The agreement is seen to be quite reasonable except, perhaps, at long times and very low Fermi levels.

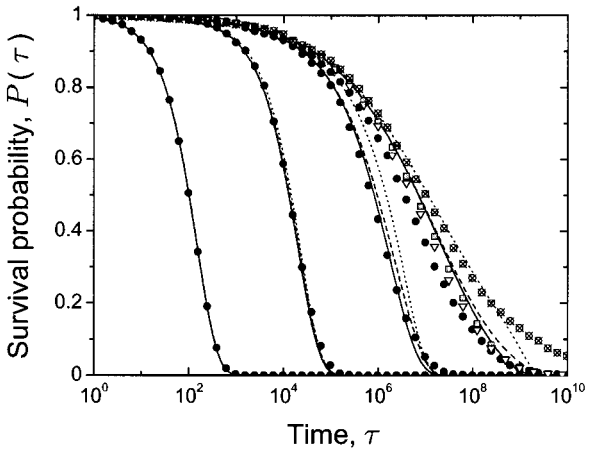

Figure 3. Cation survival probability $P(\tau)$ as a function of reduced time $\tau = k_d^0 t$ for the initial number density of cations $n_0/N = 0.002$ and different Fermi energies, $E_F = 20$, 15, 10, 5 k_BT, corresponding to the average number density of $n_d/N = 5.3\cdot10^{-4}$, $3.8\cdot10^{-3}$, 0.026, and 0.181 dark electrons, respectively (right to left). The trap energy distribution is exponential with $\alpha = 0.39$. Energy is measured with respect to the edge of the conduction band in the negative direction. Solid circles are Monte Carlo results for $N = 500$ trap sites per nanoparticle, solid lines represent the solution in the thermodynamic limit (eq 18, where Laplace inversion was performed numerically using the Crump algorithm), dotted lines correspond to eq 20, and dashed lines correspond to eq 21. Crossed open circles are Monte Carlo results obtained for $N = 500$ in the absence of dark electrons. Triangles and squares are simulation results for $N = 1000$ ($n_0 = 2$) and $N = 2000$ ($n_0 = 4$), respectively, and the Fermi energy of $E_F = 20\ k_BT$.

Deviations due to finite-size effects become negligible when N is increased. The accuracy of an approximate eq 20 also turns out to be quite good. It calls for certain improvement only when n_d is small. We can do that without loss of simplicity by expanding the first term in the expression for $K(\tau)$ in terms of n_d/N, then performing small-s expansion of $h(s)$, inverting the transform, and finally collecting the result in the form of an exponential,

$$P^{-1}(\tau) = \exp(\tau\, e^{-\epsilon_F}) + (n_0/N)\, c\, \tau^\alpha \exp[c_1 (n_d/N)\, \tau^\alpha] \quad (21)$$

where $c_1 = \Gamma(1 + \alpha)\, [\pi\alpha\, \csc(\pi\alpha)\, \Gamma(1 + 2\alpha)]^{-1}$. Equation 21 is seen to work much better.

Figure 4 illustrates the behavior of the time-dependent electron distribution function in the thermodynamic limit (see Appendix),

$$f(\epsilon, \tau) = \frac{g_F(\epsilon) + n_0\, g(\epsilon) K_1(\epsilon, \tau) \exp(-\tau\, e^{-\epsilon_F})}{1 + (n_0/N)\, K(\tau) \exp(-\tau\, e^{-\epsilon_F})} \quad (22)$$

where

$$K_1(\epsilon, \tau) = \mathcal{L}^{-1}\left[\frac{N}{(N\, h(s) - n_d)(s + e^{-\epsilon})}\right] - \frac{N}{N - n_d}\frac{\exp(\tau\, e^{-\epsilon_F})}{\exp(\epsilon_F - \epsilon) + 1} \quad (23)$$

Before the reaction actually begins, photogenerated electrons are almost equilibrated. Therefore, if the recombination rate of a conduction-band electron with a cation were slower than the trapping rate, one could consider all electrons as being equilibrated from the very start.

C. Slow Recombination. So far we assumed that the capture cross section is the same for all traps and cations. This situation

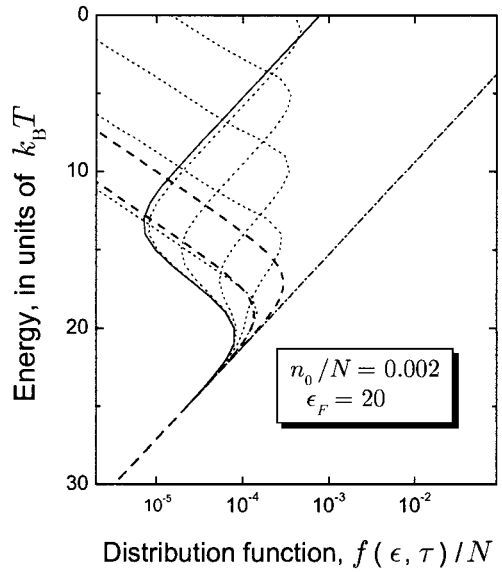

Figure 4. The calculated distribution $f(\epsilon, \tau)/N$ of electrons in the thermodynamic limit (eq 22) as a function of energy ϵ at different moments of reduced time: $\tau = k_d^0 t = 0$ (solid), 1, 10^2, 10^4, 10^6, and 10^8 (dotted, top to bottom), for the initial photogenerated electron number density of $n_0/N = 0.002$ and the Fermi energy of $E_F = 20\ k_BT$, corresponding to the number density of dark electrons $n_d/N \simeq 5 \cdot 10^{-4}$. Laplace inversion was performed numerically using the Durbin algorithm. The cation survival probability at the above moments of time is 1, 0.9995, 0.9914, 0.9418, 0.7074, and 0.1785, respectively. Dash−dotted line shows the trap energy distribution with $\alpha = 0.39$. Dashed lines are the Fermi distributions for the total electron number density at times $\tau = 10^6$ (top) and 10^8 (bottom).

seems to be realized in solar cells employing conventional organic dyes. Transient absorption studies of photoexcited xanthene dyes adsorbed on nanocrystalline TiO_2 and ZnO film have shown that the recombination rate is not sensitive to the kind of dye but strongly sensitive to the kind of semiconductor.[21] Moreover, the recombination rate of photogenerated electrons and cations was found to be similar to the rate of electron−hole recombination in a dye-free semiconductor film. This is all in agreement with what is to be expected from our theory.

Another limiting situation worth considering is where trapping is much faster than recombination. This might be the case for dyes based on Ru complex, usually employed as sensitizers in solar cells.[1] The recombination rate is much slower in such systems than in semiconductor nanoparticles sensitized with organic dyes.[21] As mentioned above, in this case all electrons are equilibrated from the very beginning. The kinetic equation for the number density n of cations reads

$$\frac{1}{n}\frac{dn}{d\tau} = -\frac{\kappa_r}{N - n_t + \kappa_r n}\int_0^\infty d\epsilon\, e^{-\epsilon} f(\epsilon, \tau) \qquad (24)$$

where κ_r is the ratio of the capture cross sections for cations and traps. By taking into account that $\kappa_r \ll 1$ and that $f(\epsilon, \tau)$ is, in fact, a Fermi distribution with a time-dependent Fermi energy $\epsilon_F(\tau)$ corresponding to the total number density of electrons n_t, eq 24 can be simplified into

$$\frac{1}{n}\frac{dn}{d\tau} = -\kappa_r e^{-\epsilon_F(\tau)}\frac{N - n_t}{N - n_t + \kappa_r n} \simeq -\kappa_r e^{-\epsilon_F(\tau)} \approx -\kappa_r c_0 (n_t/N)^{1/\alpha} \qquad (25)$$

with $c_0 = [\sin(\pi\alpha)/(\pi\alpha)]^{1/\alpha}$.

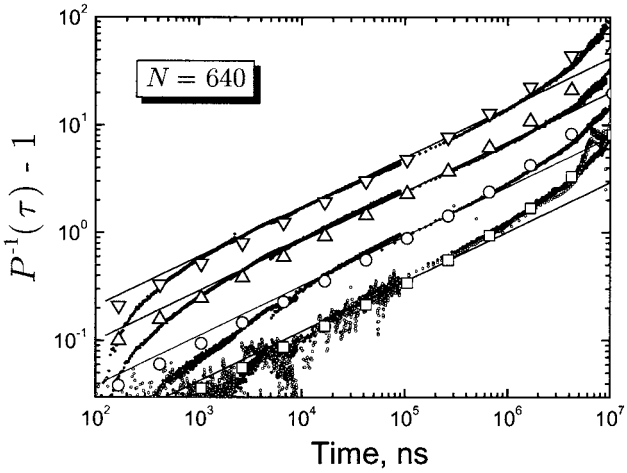

Figure 5. Transient absorption data of Haque et al.[4b] showing the decay of the cation state of $Ru(dcbpy)_2(NCS)_2$ adsorbed on a nanocrystalline TiO_2 film with an ethylene carbonate/propylene carbonate 1:1 electrolyte for different excitation intensities: 0.04 (small open circles), 0.12, 0.6, 3.5, and 6 mJ/cm^2 (full circles, from bottom). Large symbols represent numerical results obtained from eq 18 (Laplace inversion performed using the Crump algorithm) for $\epsilon_F = 17$, $k_d^0 = 1.5 \times 10^9\ s^{-1}$, $\alpha = 0.46$, and $n_0/N = 0.0016$, 0.0042, 0.011, and 0.023 (from bottom). Solid straight lines were calculated using eq 12 with $\alpha = 0.46$.

If there is no dark electron initially ($n_d = 0$), then we obtain from eq 25 for the survival probability,

$$P(\tau) = [1 + c_0\alpha^{-1}(n_0/N)^{1/\alpha}\kappa_r\tau]^{-\alpha} \qquad (26)$$

Recall that n_0 is the initial number density of photogenerated electrons (cations). Equation 26 predicts essentially the same power law type of behavior at long times, as eq 12, with the only difference that now we have $\kappa_r\tau$ instead of τ. If the number density of dark electrons is high ($n_d \gg n_0$), then the Fermi energy in eq 25 can be regarded as constant, $\epsilon_F(\tau) \simeq \epsilon_F^d$, and one obtains

$$P(\tau) = \exp(-\kappa_r\tau e^{-\epsilon_F^d}) \qquad (27)$$

This is exactly what follows from eq 20 with the difference again that τ is replaced by $\kappa_r\tau$. Simple time dependencies predicted by eqs 26 and 27 are well confirmed numerically (not shown). We may conclude that as far as the mechanism of electron motion and recombination remains the same, changing the recombination rate with respect to the trapping rate will lead to the renormalization of the time scale while the functional decay behavior will remain basically the same.

III. Comparison with Experiment

It is clear from Figures 2 and 3 that the random flight model explains, at least qualitatively, experimentally observed effects of light intensity and applied bias on the kinetics of charge recombination in TiO_2. Direct comparison with transient cation absorption data of Haque et al.[4] is shown in Figures 4 and 5. Figure 4 is presented in such a way that eq 12 gives a straight line. Recombination in an unbiased film obeys the decay law of eq 12 fairly well over a wide range of times. In our numerical calculations, we assumed that there is one photoinduced dye cation per TiO_2 nanoparticle for the excitation intensity of 0.12 mJ/cm^2 and the number of traps is $N = 640$. Deviations at short times are due to the fact that eq 12 itself is an approximation (see Figure 2). There could also be an effect of nonhomogeneous initial conditions and certain errors introduced by normalization. At the same time, one should not forget that the trap energy

distribution may differ from an exponential form, which was assumed in the absence of any better information. The long-time behavior may be different between theory and experiment for two reasons, the first one being perturbation effects by the laser pulse. Although the repitition frequency was 2 Hz, the perturbation effects are seen in all the data at times longer than 10 ms: the experimental decay curves hit zero almost linearly on a $P(t)$ versus log t plot, which is impossible. Second, even in an unbiased film there is a certain population of dark electrons. As estimated from the natural doping density of nanocrystalline TiO_2, n_d is expected to be around 0.1 per nanoparticle.[20] Even such a low density of dark electrons can lead to considerable deviations from the simple decay law of eq 12, as we have already seen in Figure 2. Indeed, eq 18 gives a much better fit to the data. Still, eq 12 is quite sufficient to characterize the general tendency.

The assumption that the interparticle migration of electrons has a negligible effect on the recombination kinetics appears to be justified experimentally: the decay becomes intensity (i.e., concentration) independent as soon as the estimated average number of photoexcited cations per nanoparticle becomes less than one. The results of Haque et al. were not obtained from a complete photoelectrochemical solar cell. In particular, a redox inactive electrolyte was used. Therefore, we are not rising an issue of photocurrent here. The initial concentration of photoexcited cations is nonuniform across the sample (it decays exponentially, according to the Beer−Lambert law). In principle, one has to average the kinetics over this concentration profile. However, as we have checked, this does not affect much any of the predicted tendencies.

The concentration dependence of the kinetics that is extracted from fitting the data to the random flight model is only in qualitative agreement with the average number of cations per nanoparticle estimated from the experimental excitation intensity. Assuming that the number of cations is proportional to the excitation intensity, one obtains $n_0 = 1$, 5, 29, and 50 for the kinetics displayed in Figure 4, whereas the fitting procedure gives $n_0 = 1$, 2.6, 6.9, and 14.4. The agreement somewhat improved when we used simulation results for fitting instead of our analytical solution. The finite-size correction is particularly important at low densities, as it is clear from Figure 2. We obtained $n_0 = 1$, 3.2, 8.6, and 16.6, respectively. One may speculate that photogeneration of cations is not proportional to the excitation intensity, as it was indeed observed in some experiments.[21] A possible source of nonlinearity is time resolution of the experimental setup. Another obvious reason is that one cannot excite more dye molecules than is actually adsorbed on the surface of a semiconductor nanoparticle. Therefore, the dependence of the number of photogenerated cations versus the excitation power should saturate at high-laser intensities. On the other hand, it is certainly possible that the above deviations are at least partially due to some deficiency of the model.

Figure 6 shows the decay data as a function of the applied bias. Although the random flight model provides a qualitative explanation of the applied bias effect on the recombination kinetics, we have not been able to fit all the data consistently with one set of parameters varying only the number of dark electrons (as Nelson et al. did for the nearest-neighbor mechanism). Either k_d^0 or α must be varied together with ϵ_F to achieve good fitting accuracy. The tendency is as if the traps were getting shallower (or the detrapping rate faster) as the Fermi energy was increased along with the bias potential. There is little point in speculating about the reason for such behavior. At this stage we feel that by incorporating the short-range

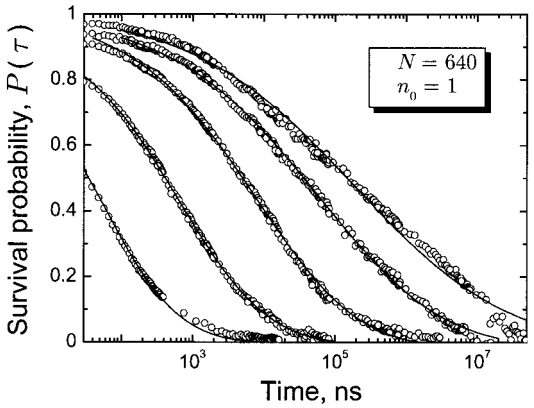

Figure 6. Transient absorption data of Haque et el.[4] showing the decay of the cation state of $Ru(dcbpy)_2(NCS)_2$ adsorbed on a nanocrystalline TiO_2 electrode with an ethanol/0.1 M tetrabutylammonium triflate electrolyte for different applied potentials: 0, 100, 200, 300, and 400 mV (circles, right to left). Lines were calculated using eq 21 for $n_0/N = 0.0016$ (one cation per nanoparticle) and $k_d^0 = 2.6 \times 10^{11}$ s^{-1}. The parameters obtained from fitting are $\alpha = 0.37$, 0.4, 0.47, 0.58, 0.81, and $\epsilon_F = 25.1$, 21.1, 17.9, 15.5, 13.1 (right to left).

transport mechanism, this inconsistency may be removed. On the other hand, the obtained value of the detrapping rate is considerably lower than that used by Nelson in her nearest-neighbor CTRW simulations.[10a] Since it is closer to a typical atomic frequency, we believe this value is more reasonable. Therefore, it is most likely that an intermediate random walk regime is realized, with a certain probability for an electron to travel a certain distance between surface trap states by diffusion in the conduction band. To rigorously confirm this conclusion, more information is necessary. In our model, the dependence of the half-time for re-reduction of the dye cation, $t_{50\%}$, defined by $P(t_{50\%}) = 1/2P(0)$, shows exactly the same power law dependence on the number of dark electrons,

$$t_{50\%} \sim n_d^{-1/\alpha} \tag{28}$$

as observed experimentally by Nelson et al.[10b] and corroborated by their nearest-neighbor random walk mechanism. To prove that one just needs to neglect the second term on the right-hand side of eq 18 (for sufficiently large n_d) and recall that $\exp(-\epsilon_F) \sim n_d^{1/\alpha}$. This coincidence leads us to suggest that it is not spatial diffusion but energy redistribution of electrons among the trap sites which governs the recombination kinetics. We shall discuss this point in more detail in the next section.

IV. Discussion

Excitation intensity dependence of the cation survival probability becomes prominent as soon as the average number of cations per nanoparticle exceeds one. This may be taken as an evidence that in experiments under discussion charge recombination is mainly an intraparticle event. The decay observed follows quite closely the power law type of kinetics with the exponent characteristic of the exponential trap energy distribution. Here we will show that this kind of behavior is determined solely by the trap energy distribution and not by the mechanism of the random walk (nearest-neighbor or random flight). A similar conclusion was reached a long time ago for an infinite 3D system,[17a] but the derivation is somewhat different in a finite system.

Let us consider a lattice of N trap sites, two of which are occupied by a geminate electron−cation pair. We fix the cation at the origin and assume that its position is in the center of

symmetry (to avoid complications arising from averaging over all possible positions, since it is not essential for our purposes). Initially, the electron is distributed uniformly over all the trap sites except the origin. Then it performs a random walk over the traps until it reaches the origin where recombination takes place instantaneously. Generalization to the case where the recombination rate is finite is straightforward.[22] Since there is no other electron which will interfere, the random walk within the MT formulation (i.e., over the sites of different energy) is equivalent to the CTRW with the waiting time distribution function $\psi(t)$ determined by averaging eq 3 over $g(E)$ of eq 1,

$$\psi(\tau) = \int_0^\infty d\epsilon\, \alpha \exp[-(1+\alpha)\epsilon - \tau e^{-\epsilon}] = \alpha\, \tau^{-1-\alpha}\, \gamma(1+\alpha, \tau) \quad (29)$$

where we used dimensionless time and energy, as before. Here $\gamma(p, x)$ is the incomplete Gamma function. The waiting time distribution function is normalized so that $\int_0^\infty d\tau\ \psi(\tau) = 1$.

The survival probability of the pair can be written as follows:

$$P(\tau) = 1 - \frac{1}{N-1}[\Phi(\tau) - 1] \quad (30)$$

where $\Phi(\tau)$ is the average number of distinct sites visited by the electron. Here $\Phi(\tau) - 1$ gives the number of sites where the electron can potentially find the cation (i.e., all sites except the starting site), and $1/(N-1)$ is the probability to find the cation in each of those sites. This quantity $\Phi(\tau)$ received much attention in the random walk theory, and it is well known how it is expressed in terms of the so-called random walk generating function, $G(\mathbf{r}, z)$:[23]

$$\hat{\Phi}(s) = \frac{\hat{\psi}(s)}{s\,[1-\hat{\psi}(s)]\, G[0, \hat{\psi}(s)]} \quad (31)$$

where we used the same notation for the Laplace transform as before. Obviously, at time zero $\Phi(0) = 1$ and $P(0) = 1$, while at infinity $\Phi(\infty) = N$ and $P(\infty) = 0$.

One can analyze the long-time behavior of $P(\tau)$ even without any structural information about the lattice. We only need to use the fact that our lattice is finite and thus[23]

$$G(0, z) = \frac{1}{N(1-z)} + g(0, z) \quad (32)$$

that is, we explicitly remove the singularity. Thus, we can rewrite eq 31 as follows:

$$\hat{\Phi}(s) = \frac{1}{s}\frac{N\,\hat{\psi}(s)}{1 + N\,[1-\hat{\psi}(s)]\, g[0, \hat{\psi}(s)]} \quad (33)$$

Now we need small s expansion of $\hat{\psi}(s)$,

$$\hat{\psi}(s) = \frac{1}{s}\frac{\alpha}{1+\alpha}\, {}_2F_1(1, 1+\alpha; 2+\alpha; -1/s) = 1 - s^\alpha \pi\alpha \csc(\pi\alpha) + \mathcal{O}(s) \quad (34)$$

Simple algebraic manipulations lead to

$$\hat{P}(s) = \frac{1}{s}\frac{N\, g(0,1)\, s^\alpha \pi\alpha \csc(\pi\alpha)}{1 + N\, g(0,1)\, s^\alpha \pi\alpha \csc(\pi\alpha)} \quad (35)$$

Equation 35 shows that at very long times (very small s), one can neglect the second term and finally obtain

$$P(\tau) \simeq N\, g(0,1)\, \Gamma(1+\alpha)\, \tau^{-\alpha} \quad (36)$$

This is what we wanted to show: the long-time behavior of the recombination kinetics is determined solely by the trap energy distribution, while all the structural information about the lattice and the random walk mechanism enters as a numerical prefactor (regular part of the random walk generating function).

Equation 36 is consistent with eq 12 derived for the random flight model. It is known that in the nearest-neighbor random walk, $g(0, 1)$ is sensitive to the lattice dimensionality.[23] In three dimensions, $g(0, 1)$ approaches a constant close to unity as $N \to \infty$, while for 2D systems it grows as ln N. Preliminary calculations on periodic cubic lattices show that for N of about several hundred, typical of TiO_2 nanoparticles, the values of $g(0, 1)$ are very similar both for the nearest-neighbor walk in 3D or 2D and for the random flight. This simple analysis confirms the earlier conclusion that what governs the recombination kinetics is diffusion not in the usual configurational space but in the energy space (energy redistribution).[4,10b] The random flight model is the simplest one which accounts for the energy redistribution. It does not require simulations to explain the trap-filling effect (unlike the nearest-neighbor random walk model). Therefore, we hope that it will be useful for qualitative estimations before detailed simulations for a more realistic mechanism are carried out.

In contradiction to the experimental results of Haque et al. discussed above, Bauer et al.[24] have recently reported that the electron−cation recombination kinetics for the same dye molecule (i.e., $Ru(dcbpy)_2(NCS)_2$) adsorbed on the surface of TiO_2 and ZnO is biexponential with rather large time constants of 300 ns and 2.6 μs, independent of the light intensity and practically independent of the kind of semiconductor. The observed high recombination rate independent of the excitation intensity could, in principle, be rationalized if the intensity was high and the number of photogenerated cations was saturated. However, the lowest intensities employed are <0.5 mJ/cm^2 indicating that this is probably not the case. Independence of the recombination rate of the kind of semiconductor material could be explained if the reaction was limited by direct long-range electron transfer from the trap site nearest to the cation, not via the conduction band. This would also explain exponentiality of the kinetics. However, the observed decays are perhaps too fast to corroborate such a mechanism; much slower decays were observed by Haque et al., and in their experiments, the kinetics were quite dispersive indicating that energy redistribution of electrons over the traps sites (inherent to a given semiconductor material) is important in influencing the recombination process. More experiments are needed to resolve this puzzle.

Acknowledgment. We are grateful to Prof. J. R. Durrant and Drs. S. A. Haque and Y. Tachibana for providing us with their experimental data. We would also like to thank Dr. R. Katoh for helpful discussions on the details of a transient absorption measurement in semiconductor nanoparticles and for informing us of his experimental results prior to publication.

Appendix

To solve eq 5, we consider the normalized distribution function,

$$\varphi(\epsilon, \tau) = f(\epsilon, \tau)/n(\tau) \quad (A1)$$

The kinetic equation for $\varphi(\epsilon,\tau)$ is linear,

$$\frac{\partial}{\partial\tau}\varphi(\epsilon,\tau) = -e^{-\epsilon}\varphi(\epsilon,\tau) + g(\epsilon)\,\Phi(\tau) \tag{A2}$$

where

$$\Phi(\tau) = \int_0^\infty d\epsilon\, e^{-\epsilon}\varphi(\epsilon,\tau) \tag{A3}$$

Equation 7 modifies into

$$\frac{1}{n^2}\frac{dn}{d\tau} = -\frac{1}{N}\Phi(\tau) \tag{A4}$$

Equation A2 can be solved in terms of $\Phi(\tau)$ by using Laplace transformation. As a result, we obtain

$$\hat{\Phi}(s) = h^{-1}(s) - 1 \tag{A5}$$

where

$$h(s) = s\int_0^\infty d\epsilon\,\frac{g(\epsilon)}{s+e^{-\epsilon}} \tag{A6}$$

The above integral can be represented in terms of the hypergeometric function,[25] as defined in the main text. Equation 8 follows directly from eq A4, with $\hat{K}(s) = \hat{\Phi}(s)/s$.

In the presense of dark electrons, the solution is quite similar. By using the auxiliary distribution function of eq A1, we are led to a linear master equation A2 and a kinetic equation A4, but with

$$\Phi(\tau) = \frac{N}{N-n_d}\int_0^\infty d\epsilon\, e^{-\epsilon}\varphi(\epsilon,\tau) \tag{A7}$$

The survival probability of cations is expressed in terms of $\Phi(\tau)$ exactly in the same way as before, that is,

$$P^{-1}(\tau) = 1 + \frac{n_0}{N}\int_0^\tau dx\,\Phi(x) \tag{A8}$$

but $\Phi(\tau)$ is now different and the initial condition is different (see eq 16). Solution of eq A2 in terms of $\hat{\Phi}(s)$ yields,

$$\hat{\Phi}(s) = \left(\frac{1}{n_0}\int_0^\infty d\epsilon\,\frac{e^{-\epsilon}f(\epsilon,0)}{s+e^{-\epsilon}}\right)\left[h(s) - \frac{n_d}{N}\right]^{-1} \tag{A9}$$

and after integration,

$$\hat{\Phi}(s) = \frac{N}{Nh(s)-n_d} - \frac{N}{N-n_d} + \left(\frac{N}{n_0} - \frac{N}{N-n_d}\right)\frac{1}{s\,e^{\epsilon_F}-1} \tag{A10}$$

Equation 18 is obtained by Laplace inversion and minor rearrangement. The distribution function in eq 22 is calculated by noticing the Laplace relationship following from eq A2,

$$\hat{\varphi}(\epsilon,s) = \frac{f(\epsilon,0)/n_0 + g(\epsilon)\,\hat{\Phi}(s)}{s+e^{-\epsilon}} \tag{A11}$$

References and Notes

(1) (a) O'Regan, B.; Grätzel, M. *Nature* **1991**, *353*, 737. (b) Hagfeldt, A.; Grätzel, M. *Chem. Rev.* **1995**, *95*, 49. (c) *Acc. Chem. Res.* **2000**, *33*, 269.

(2) Tachibana, Y.; Haque, S. A.; Mercer, I. P.; Durrant, J. R.; Klug, D. R. *J. Phys. Chem. B* **2000**, *104*, 1198.

(3) (a) Yan, S.; Hupp, J. T. *J. Phys. Chem.* **1996**, *100*, 6867. (b) Liu, D.; Fessenden, R. W.; Hug, G. L.; Kamat, P. V. *J. Phys. Chem. B* **1997**, *101*, 2583. (c) Argazzi, R.; Bignozzi, C. A.; Heimer, T. A.; Castellano, F. N.; Meyer, G. J. *J. Phys. Chem. B* **1997**, *101*, 2591. (d) Martini, I.; Hodak, J. H.; Hartland, G. V. *J. Phys. Chem. B* **1998**, *102*, 607.

(4) (a) Haque, S. A.; Tachibana, Y.; Klug, D. R.; Durrant, J. R. *J. Phys. Chem. B* **1998**, *102*, 1745. (b) Haque, S. A.; Tachibana, Y.; Willis, R. L.; Moser, J. E.; Grätzel, M.; Klug, D. R.; Durrant, J. R. *J. Phys. Chem. B* **2000**, *104*, 538.

(5) Schwarzburg, K.; Willig, F. *Appl. Phys. Lett.* **1991**, *58*, 2520.

(6) (a) Sodergren, S.; Hagfeldt, A.; Olsson, J.; Lindquist, S.-E. *J. Phys. Chem.* **1994**, *98*, 5552. (b) Solbrand, A.; Lindström, H.; Rensmo, H.; Hagfeldt, A.; Lindquist, S.-E.; Södergren, S. *J. Phys. Chem. B* **1997**, *101*, 2514.

(7) (a) Huang, S. Y.; Schlichthörl, G.; Nozik, A. J.; Grätzel, M.; Frank, A. J. *J. Phys. Chem. B* **1997**, *101*, 2576. (b) Schlichthörl, G.; Huang, S. Y.; Sprague, J.; Frank, A. J. *J. Phys. Chem. B* **1997**, *101*, 8141. (c) van de Lagemaat, J.; Park, N.-G.; Frank, A. J. *J. Phys. Chem. B* **2000**, *104*, 2044.

(8) (a) Dloczik, L.; Ileperuma, O.; Lauermann, I.; Peter, L. M.; Ponomarev, E. A.; Redmond, G.; Shaw, N. J.; Uhlendorf, I. *J. Phys. Chem. B* **1997**, *101*, 10281. (b) Peter, L. M.; Ponomarev, E. A.; Franco, G.; Shaw, N. J. *Electrochim. Acta* **1999**, *45*, 549. (c) Franco, G.; Gehring, J.; Peter, L. M.; Ponomarev, E. A.; Uhlendorf, I. *J. Phys. Chem. B* **1999**, *103*, 692.

(9) (a) Jongh, P. E.; Vanmaekelbergh, D. *J. Phys. Chem. B* **1997**, *101*, 2716. (b) Vanmaekelbergh, D.; van Pieterson, L. *Phys. Rev. Lett.* **1998**, *80*, 821. (c) Vanmaekelbergh, D.; Jongh, P. E. *J. Phys. Chem. B* **1999**, *103*, 747.

(10) (a) Nelson, J. *Phys. Rev. B* **1999**, *59*, 15374. (b) Nelson, J.; Haque, S. A.; Klug, D. R.; Durrant, J. R. *Phys. Rev. B* **2001**, *63*, 205321.

(11) Usami, A.; Ozaki, H. *J. Phys. Chem. B* **2001**, *105*, 4577.

(12) Cao, F.; Oskam, G.; Mayer, G. J.; Searson, P. C. *J. Phys. Chem.* **1996**, *100*, 17021.

(13) (a) Schmidlin, F. W. *Phys. Rev. B* **1977**, *16*, 2362. (b) Noolandi, J. *Phys. Rev. B* **1977**, *16*, 4474.

(14) Rudenko, A. I.; Arkhipov, V. I. *Philos. Mag. B* **1982**, *45*, 177; 189; 209.

(15) Adriaenssens, G. J.; Baranovskii, S. D.; Fuhs, W.; Jansen, J.; Öktü, Ö. *Phys. Rev. B* **1995**, *51*, 9661.

(16) Scher, H.; Montroll, E. W. *Phys. Rev. B* **1975**, *12*, 2455.

(17) (a) Blumen, A.; Klafter, J.; Zumofen, G. *Phys. Rev. B* **1983**, *27*, 3429. (b) Blumen, A.; Zumofen, G.; Klafter, J. *Phys. Rev. B* **1984**, *30*, 5379.

(18) Miller, A.; Abrahams, E. *Phys. Rev.* **1960**, *120*, 745.

(19) Poumellec, B.; Marucco, J. F.; Lagnel, F. *Phys. Status Solidi A* **1985**, *89*, 375.

(20) Rothenberger, G.; Fitzmaurice, D.; Grätzel, M. *J. Phys. Chem.* **1992**, *96*, 5983.

(21) (a) Katoh, R., unpublished results (2001); (b) Hara, K.; Horiuchi, H.; Katoh, R.; Singh, L. P.; Sugihara, H.; Sayama, K.; Murata, S.; Tachiya, M.; Arakawa, H. *J. Phys. Chem. B* **2002**, *106*, 374.

(22) Barzykin, A. V.; Tachiya, M. *Phys. Rev. Lett.* **1994**, *73*, 3479.

(23) Weiss, G. H. *Aspects and Applications of the Random Walk*; North-Holland, Amsterdam: 1994.

(24) Bauer, C.; Boschloo, G.; Mukhtar, E.; Hagfeldt, A. *J. Phys. Chem. B* **2001**, *105*, 5585.

(25) Abramowitz, M.; Stegun, I. A. *Handbook of Mathematical Functions*, Dover: New York, 1970.